Supplemental Information

Supplemental Figure Legends

Figure S1. Reversible inhibition of contractility and transcriptional suppression of LMNA result in increased DNA damage, Related to Figures 1 & 2.

(A) **(*i*)** Full-length Western blot (top) and corresponding Coomassie Brilliant Blue-stained gel (bottom) for data shown in Fig.1B&C. Key time points are highlighted in colors. **(*ii*)** Densitometry line profiles along the electrophoresis axis (vertical colored arrows) shows significant changes in LMNA and γH2AX, but not β-actin (loading control). **(*iii*)** Coomassie Brilliant Blue total intensity along each lane shows total protein content remains unchanged across conditions. All error bars indicate ±SEM.

(B) **(*i*)** WB for a key time point (1h post-blebb treatment) using an alternative housekeeping protein HSP90 as a loading control (top). Densitometry line profiles (bottom) show similar ~35% reduction in LMNA but not HSP90, even in the presence of a protein synthesis inhibitor, (CHX, or 'Trx-i'). **(*ii*)** Coomassie Brilliant Blue total intensity remains unchanged (<10%) across conditions (n=8 hearts per lysate).

(C) Mass spectrometry (MS) of heart lysates detects 29 peptides unique to LMNA, and verifies that a broad range of housekeeping proteins, including LMNB1, LMNB2, GAPDH, HSP70, β-tubulin, and β-actin, remain unchanged with blebbistatin treatment (± Trx-i). n=8 hearts per lysate.

(D) **(*i*)** Quantification of tissue beating strain $\Delta AR/AR_{ref}$ and **(*ii*)** heart rate (beats / min; BPM) in blebbistatin treated hearts. Myosin-II inhibition by blebbistatin rapidly suppresses beating (<30 min), but effects are reversible such that washout of drug with culture medium (± OM) results in near full recovery by 1h.

(E) **(*i*)** LMNA and γH2AX immunoblots with different doses of MO. **(*ii*)** Low dowses (<5 μm) have no significant effect on beating strain ($\Delta AR/AR_{ref}$) or rate (BPM), but higher doses suppress beating, indicating potential cytotoxicity (one-way ANOVA; *p<0.05, **<0.01).

(F) **(*i*)** Retinoic acid (RA) and antagonist to retinoic acid (AGN) treatment in intact embryonic hearts have no observable effect on LMNA levels or DNA damage (γH2AX) at 3h. (n=6 hearts per cond.). **(*ii*)** Significant changes in LMNA and γH2AX are detectable only after 72h treatment, consistent with slow transcriptional modulation. A reduction in LMNA upon RA treatment (72h) is accompanied by an increase in DNA damage as measured by γH2AX, while AGN treatment leads to an upregulation of LMNA coupled to suppression of DNA damage (n=8 hearts per lysate, t-test; *p<0.05).

(G) LMNA WB of RA/AGN treated E4 hearts, with three different loading volumes (Low, Med, High). Bottom left: LMNA vs HSP90 scatter plot (all $R^2 > 0.99$); Right: linear fits from LMNA vs HSP90 scatter plot show slopes for AGN > Untr. > RA.

(H) RA and AGN treatment does not significantly affect contractility of hearts even after 72h of treatment.

Figure S2. Suppression of LMNA levels in intact embryonic hearts and in beating hiPS-CMs increase rupture under high stress, causing prolonged (>1h) loss of repair factors from the nucleus and accumulation of DNA damage, Related to Figure 3.

(A) **(*i*)** Blebbistatin treatment and washout have no significant effect on cell death/viability, as determined by %-transfected cells with fragmented DNA. **(*ii*)** As with embryonic hearts, blebbistatin washout results in an increase in rupture with cytoplasmic mis-localization of KU80. An excess of rupture is seen with washout plus a nuclear import inhibitor (ivermectin, 'Imp-i', which inhibits Impα/β mediated import), but not with washout plus a specific inhibitor of integrase(IN) nuclear import (mifepristone, 'Mifepr.') that does not target KU80's NLS. On the other hand, washout with a nuclear export inhibitor (leptomycin B, 'Exp-I') greatly suppresses cytoplasmic mis-localization of KU80 (t-test *p<0.05, **<0.01). All error bars indicate ±SEM.

(B) As seen with nuclei in intact embryonic hearts, 'nuclear beating' occurs in hiPS-CMs and can be quantified by changes in nucleus area and DNA mean intensity (condensation/de-condensation of DNA), which are inversely correlated.

(C) Time-lapse images of nuclei probed with a pointed (<1 μm) Atomic Force Microscopy (AFM) tip (at ~7 nN). Nuclear rupture upon stress is evident in the rapid and stable accumulation of a cytoplasmic protein that binds DNA (GFP-cGAS).

(D) **(*i*)** Nuclear/cytoplasmic KU80 IF intensity ratio decreases with siLMNA knockdown, and **(*ii*)** anti-correlates with γH2AX foci count (one-way ANOVA; ***p<0.001).

(E) **(*i*)** Cytoplasmic mis-localization is not limited to KU80, but applicable to other DNA repair factors including 53BP1 and RPA2 (top: IF images, bottom: intensity profiles along white dashed line). Scale bar = 10 μm. **(*ii*)** Time-lapse images of siLMNA knockdown cells transduced with GFP-53BP1 show that nuclear rupture and cytoplasmic mis-localization occur within minutes and are maintained for at least 1h in culture indicating slow recovery.

(F) Total (nuclear + cytoplasmic) KU80 abundance is unaffected by siLMNA or blebbistatin treatment.

(G) Kymograph of beating hiPS-CM organoids generated by tracing length along yellow line with time. Blebbistatin treatment results in reversible inhibition of contractility.

Figure S3. Repair factor loss perturbs cell cycle, but effects are rescued by myosin-II inhibition, Related to Figure 4.

(A) **(*i*)** Histograms of normalized DNA content in hiPS-CMs after knockdown of LMNA and DNA repair factors. All repair factor knockdowns results in a higher fraction of '4N' cells, with effects most severe for siCombo. **(*ii*)** Kolmogrov-Smirnov test (α = 0.05) for siRNA treated populations. **(*iii*)** γH2AX foci count inversely correlates with KU80 nuclear IF intensity at the single cell level, consistent with limited repair. All error bars indicate ±SEM.

(B) DNA damage per total DNA is elevated in 4N cells after LMNA knockdown and decreased in 2N cells, based again on measurements of individual cells.

(C) Left: Representative scatter plot of EdU intensity versus total DNA content used to determine cell cycle phase (G1, S, and G2). Right: siLMNA treatment increases fraction of cells in G2, but effects are rescued by blebbistatin (t-test *p<0.05, ***<0.001).

(D) **(*i*)** Venn diagram of nuclear proteins pulled down by co-immunoprecipitation mass spectrometry (CoIP-MS) using anti-GFP on GFP-KU70 expressing cells. **(*ii*)** As expected, KU80 is a strong interaction partner of KU70 (as components of the KU complex), as are lamins-A and B.

Figure S4. Parallel increases in lamin-A:B, collagen matrix, and tissue stiffness fit a 'lose it or use it' model of tension-stabilization of fibers, Related to Figure 5.

(A) LMNA MS intensity scales with heart tissue stiffness with exponent α ~ 0.75 similar to that for adult tissue proteomes (Swift, et al., 2013). All error bars indicate ±SEM.

(B) Lamins-B1 & B2 remain comparatively constant throughout development and exhibit much weaker scaling (α < 0.25).

(C) Heartmap of proteins detected by LC-MS/MS in the ECM, adhesion complexes, sarcomeres, and the nuclear lamina. Proteins were ranked based on the fold-change relative to the average.

(D) Lamin-A:B ratio quantified by **(*i*)** WB densitometry and **(*ii*)** IF (t-test *p<0.05).

(E) MS measurements of collagen-I calibrated with spike-ins of known amounts of purified collagen-I. Dividing calibrated measurements by reported myocardium volumes (Kim, et al., 2011) gives collagen-I densities far lower than those used in studies of collagen-I gels (Yang, et al., 2009), suggesting lower densities are needed for a stiffness in the kPa range as measured for heart (Fig.4C-*ii*).

(F) Heart stiffness measurements by micropipette aspiration plotted against collagen-I MS intensity yield power-law scaling comparable to that found for diverse adult tissues (Swift, et al., 2013).

(G) LMNA & B immunoblots for E10 brain and liver tissue.

Figure S5. Acute drug perturbations in E4 heart rapidly impact LMNA levels and phosphorylation at multiple sites, but do not affect total abundance of repair factors or MMP2, Related to Figure 5.

(A) Immunoblot validation of LMNA trends seen in MS profiling of drug perturbations (n>6 hearts per lysate). Immunoblots against phosphorylated Ser22 and Ser390 show that normalized phosphorylation ('pSer22/LMNA' and 'Ser390/LMNA') increases with blebbistatin-inhibition of actomyosin stress or with collagenase-softening of tissue, but decreases with CDK-i treatment (one-way ANOVA; **p*<0.05, ** *p*<0.01, ****p*<0.001). All error bars indicate ±SEM.

(B) **(*i*)** RPA1 (DNA repair factor) and **(*ii*)** pro-MMP2 levels are unaffected by drug perturbations (per MS). **(*iii*)** Catalytic activation of MMP2 ('cleaved/pro-MMP2' fraction, as measured by immunoblot) is not affected by drug perturbations to contractility and/or collagen matrix.

(C) Schematic plot of fractional abundance of intact LMNA and its phosphorylated fragments, including intermediates, upon relaxation of stress.

Figure S6. Cell-on-gel morphological trends in CM size, shape, contractility, and LMNA mirror those of *in vivo* hearts without affecting cell cycle/proliferation, Related to Figure 6.

(A) **(*i*)** Projected area of the nucleus relative to that of the cell ('Nucl./Cyto. Area fraction') decreases **(*ii*)** and cells elongate (increased aspect ratio, AR), as the embryonic heart stiffens and cells undergo hypertrophic growth and spreading from E4 – E10. Isolated E4 CMs cultured on gels likewise exhibit increased cell spreading and elongation on stiffer gels (t-test **p*<0.05, **<0.01, ***<0.001). All error bars indicate ±SEM.

(B) Two of the most abundantly expressed α- and β-tubulin isoforms (TUBA1C, TUBB7) increase in level from E4 to E10 and the increase is accompanied by a decrease in TTLL12, which tyrosinates and de-stabilizes microtubules (Robison, et al., 2016). Trends are consistent with increased stiffness as well as with polarization/elongation of CMs during development (Fig.4D-*ii*, Fig.S6A).

(C) Axial alignment of cells (anisotropy, quantified as 1/COV of the major axes of nuclei) increases from early (E4) to late (E11) hearts. Upper left inset: major axis angle distribution of E4 and E11 nuclei.

(D) Nuclear volume (estimated by confocal Z-stack) decreases in development from E4 to E10.

(E) Varying matrix stiffness alone in E4 CM cultures is sufficient to recapitulate trends in morphology and intracellular organization seen *in vivo* (from E4 to E11).

(F) Normalized cell and nuclear beating strains measured by **(*i*)** '$\Delta AR/AR_{ref}$' and **(*ii*)** '$\Delta Area/Area_{ref}$', and **(*iii*)** %-beating cells all exhibit an optimum on gels mimicking the stiffness of embryonic hearts (~2 kPa). Blebbistatin treatment abolishes mechano-sensitivity. (n>10 cells/nuclei per condition).

(G) **(*i*)** Nuclear beating strain ('Nucleus $\Delta AR/AR_{ref}$') correlates well with cell beating strain ('Cell $\Delta AR/AR_{ref}$'), **(*ii*)** but lamin-A:B ratio does not correlate with beating. Lamin-A:B instead couples to average morphology changes in spreading area and elongation that relate to basal isometric tension.

(H) Lamin-A:B in cells on rigid plastic decreases with MYK inhibition of cardiac myosin contractility (as with blebbistatin treatment), but remains unchanged with OM treatment.

Figure S7. Phosphorylation of LMNA favors degradation by MMP2, Related to Figure 6 & 7.

(A) Representative images of cells transduced with phsopho-mimetic mutants GFP-S22A and GFP-S22E, with or without protein synthesis inhibitor Trx-i. **(*i*,*ii*)** Line profiles across individual nuclei reveal 'non-phosphorylatable' GFP-S22A signal is far more enriched at the lamina than in the nucleoplasm, compared to 'constitutively phosphorylated' GFP-S22E (n>15 nuclei). Treatment with Trx-i does not alter nucleoplasm/lamina ratio in either mutant. **(*iii*)** Overall fluorescence intensity of GFP-S22A is ~50% higher than that of GFP-S22E. Trx-i induces a minor ~10% decrease in either case. All error bars indicate ±SEM.

(B) Immunoblots with anti-lamin-A/C and anti-GFP reveal multiple low-MW degradation fragment bands (green triangles) in the GFP-S22E mutant which are absent in the S22A mutant. **(*ii*)** Line intensity profile of anti-lamin-A/C immunoblot (*i*, left). Low-MW degradation fragments that are present in the GFP-S22E mutant but not in the GFP-S22A mutant, are shaded in blue, with green arrows indicating distinct bands.

(C) GFP fluorescence intensity of GFP-S22E expressing cells increases upon MMP2-I (ARP-100) treatment, consistent with inhibition of degradation.

(D) Representative transcriptomics dataset for mouse embryonic hearts obtained from NCBI's Gene Expression Omnibus (GEO) Database. Log-log plot shows normalized mRNA expression vs *Col1a1*. As expected for obligate heterotrimer subunits of collagen-I, *Col1a2* correlates robustly with *Col1a1*, with scaling exponent (= slope on a log-log plot), $\alpha_{Col1a2} \sim 1$. Lmna also increases with *Col1a1*, although with slightly weaker scaling $\alpha_{Lmna} \sim 0.3$, indicating potential feedback to gene expression. Right: bar graph of average scaling exponents (vs *Col1a1*) for proteins of interest in the ECM, cytoskeleton, nuclear envelope, as well as several transcription factors implicated in mechanosensing and/or cardiac development.

(E) Proteomics dataset for diverse E18 chick embryonic tissues, adapted from Uebbing et al. (Uebbing et al., 2015). Lmna again increases with Col1a1&2, with exponent $\alpha_{Lmna} \sim 0.3$. Right inset: datapoints for heart samples plotted separately reveal similar scaling.

(F) Tissue-dependent timing of initial LMNA expression in early embryos correlates well with the stiffness that a given tissue eventually achieves in adult (adapted from (Swift, et al., 2013; Rober, et al., 1989)).

Figure S1

Mass Spec. confirms WB quantitation of LMNA & DNA damage,
and reveals housekeeping proteins (including LMNB's) remain unchanged with actomyosin perturbations

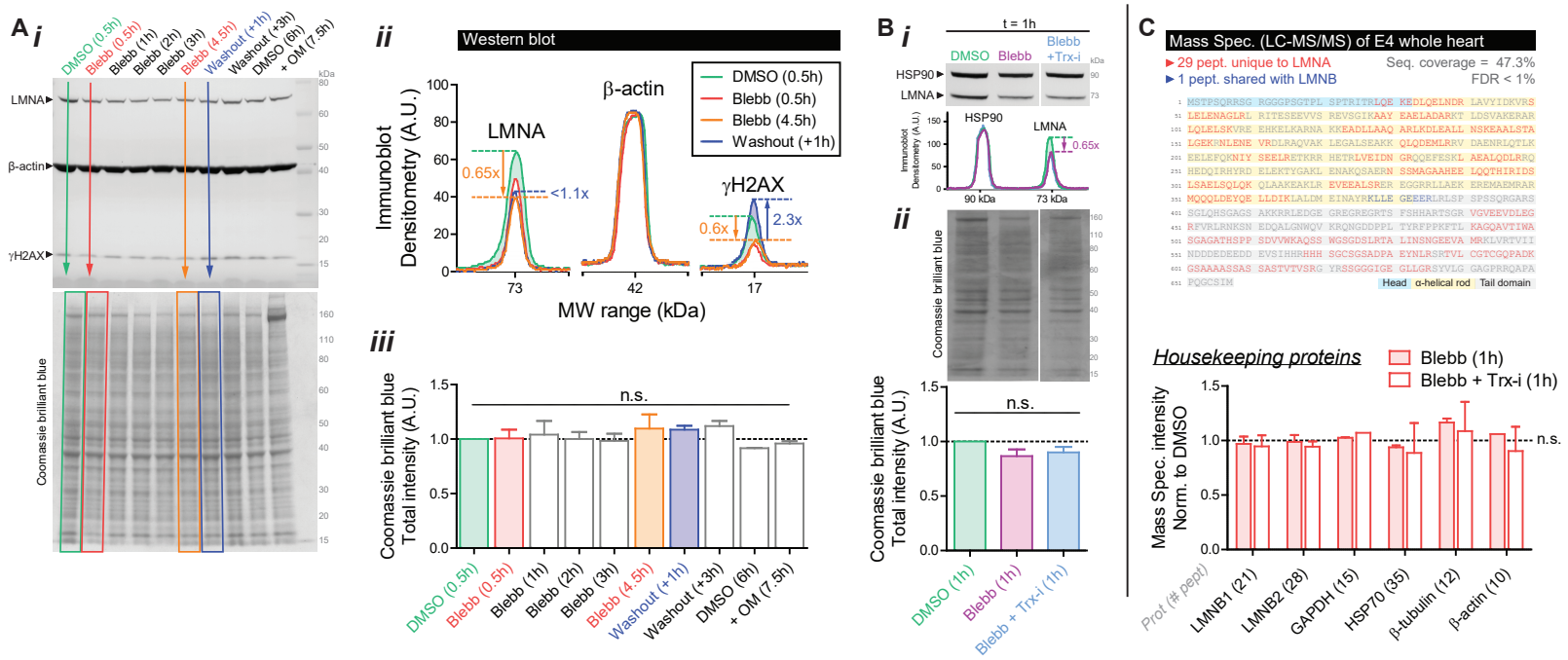

Beating is rapidly perturbed by myo-II modulators but not by low doses (<5uM) of MO treatment

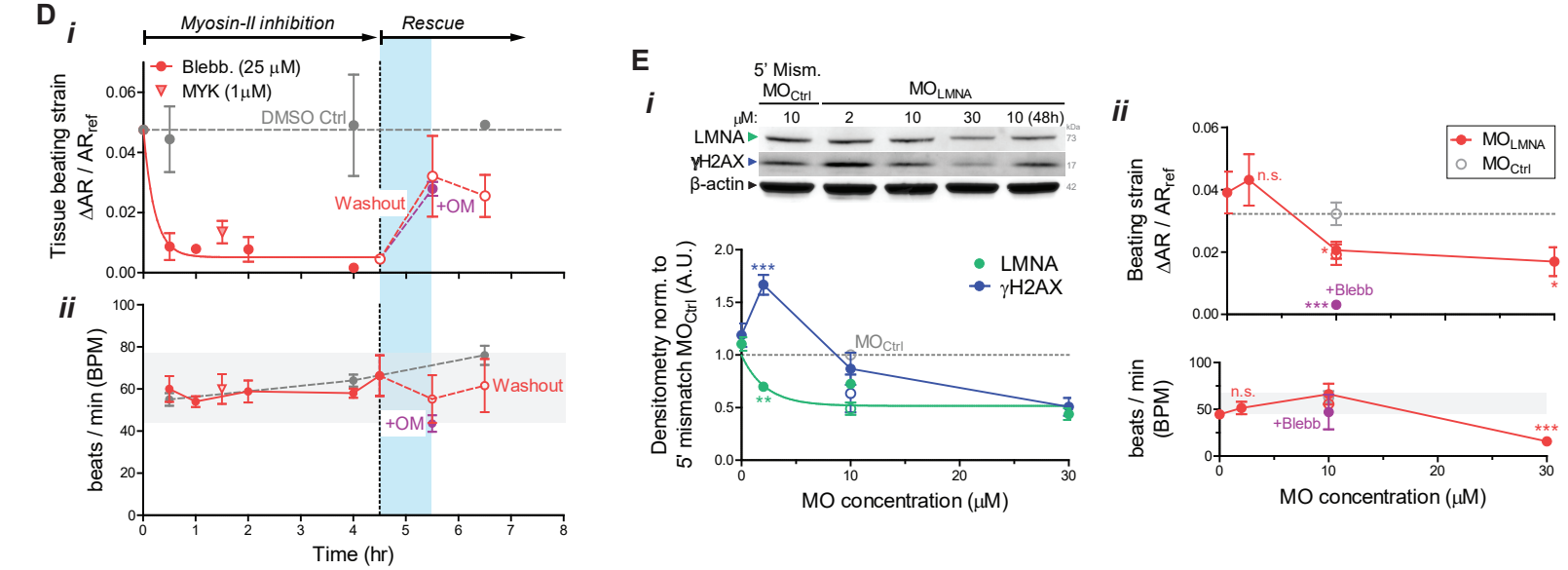

Transcr. regulation by RA or AGN result in anti-correlated changes in LMNA and DNA damage after days of treatment

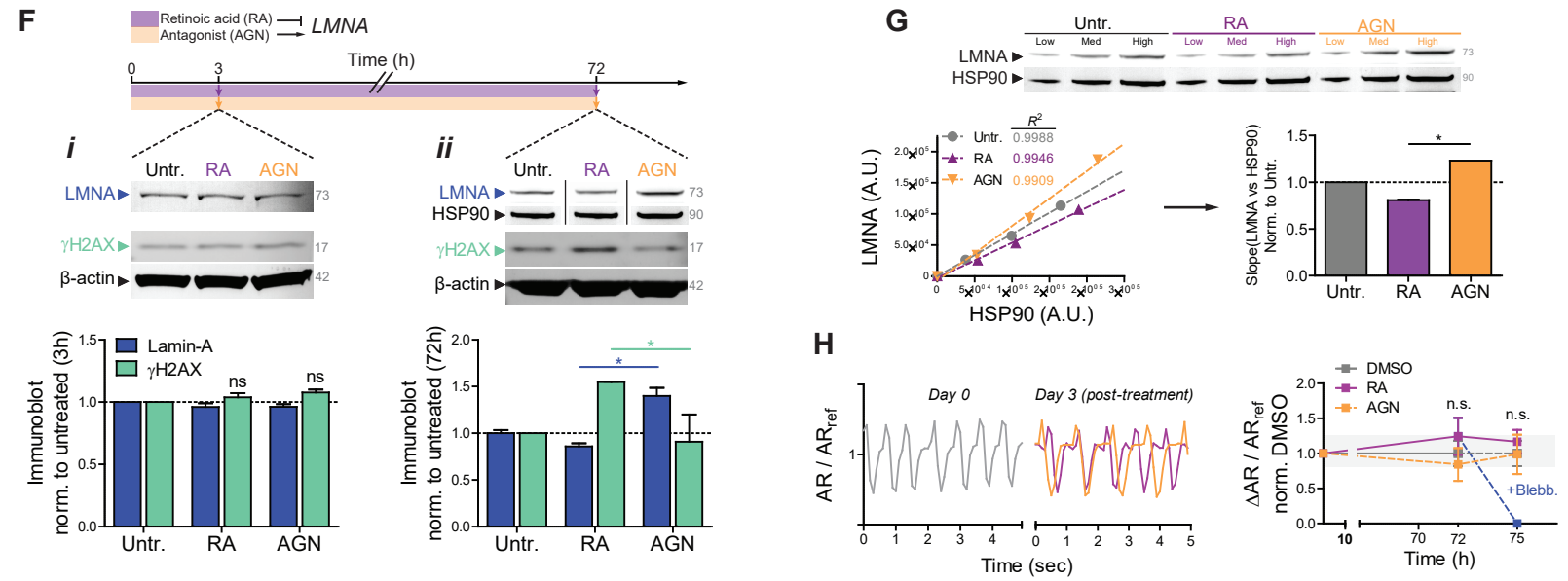

Figure S2

LMNA KD or AFM probing of nuclei cause mis-localization of multiple repair factors, which persists for ~hours

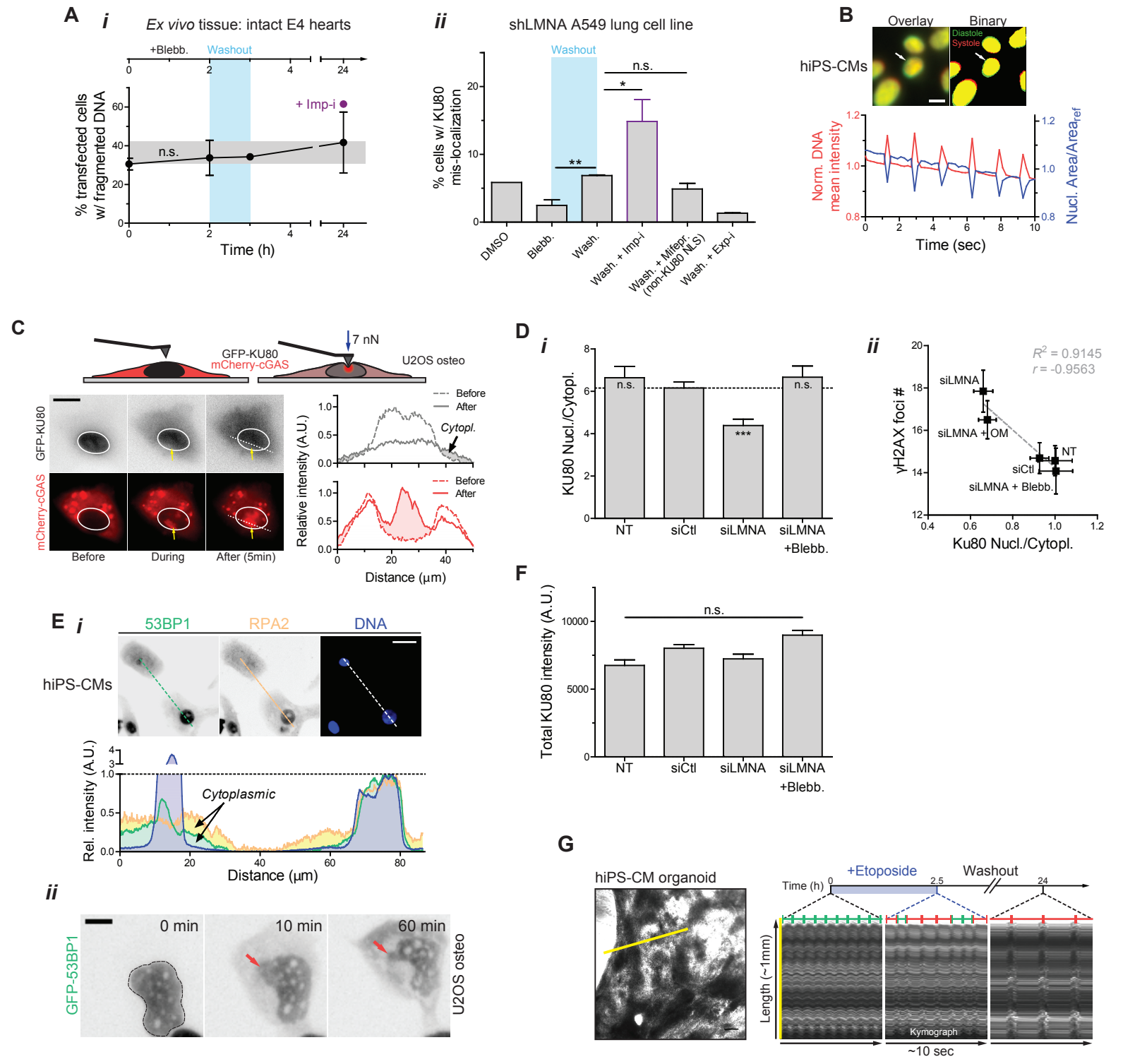

Figure S3

KD of LMNA or repair factors causes increased DNA damage with accumulation in late cell cycle; rescue by blebbistatin

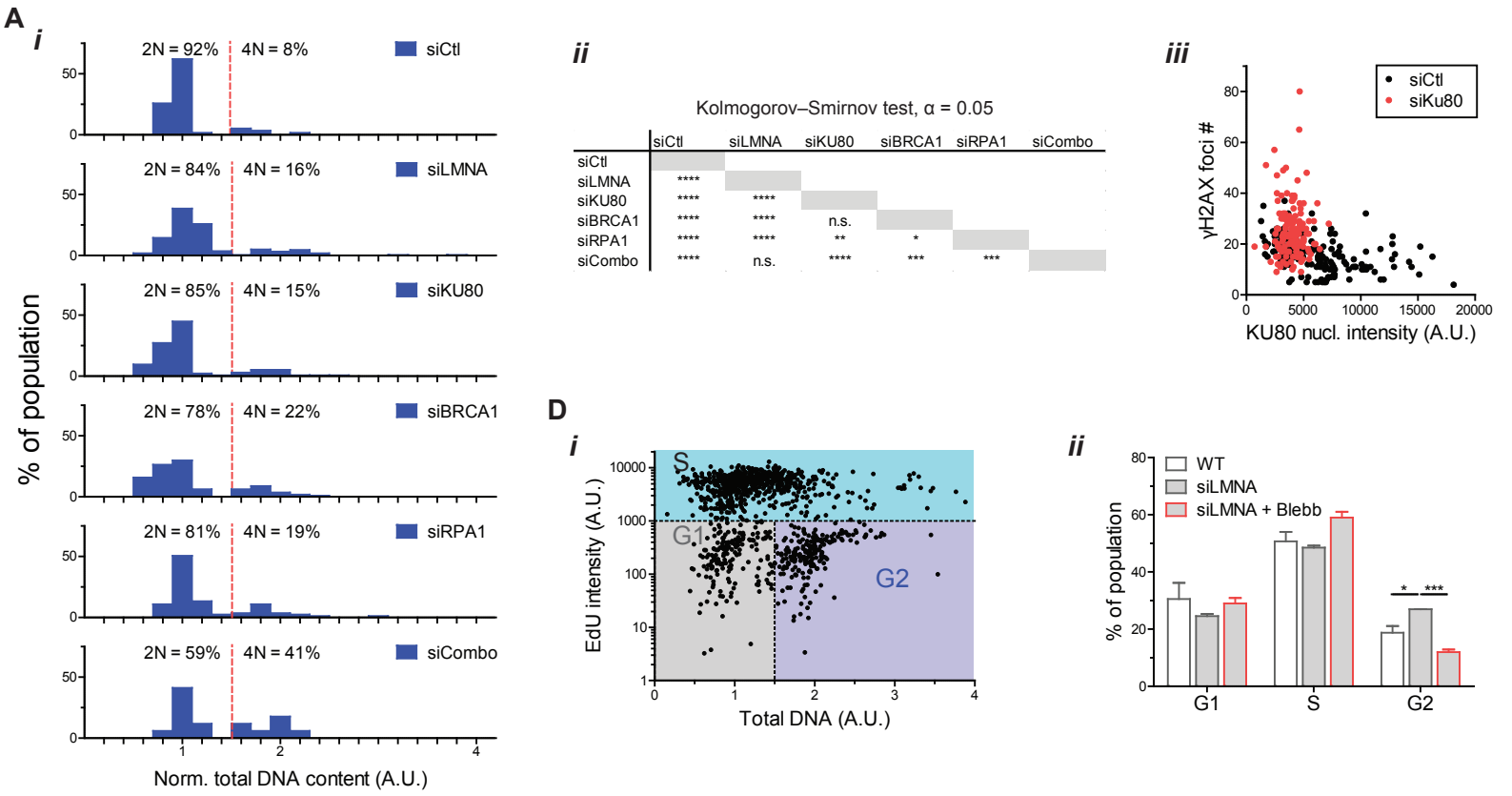

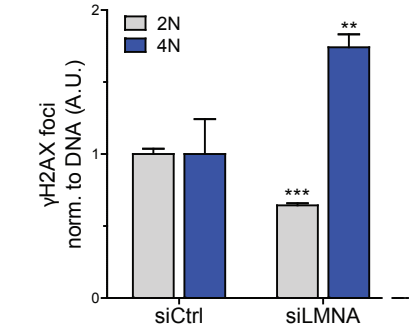

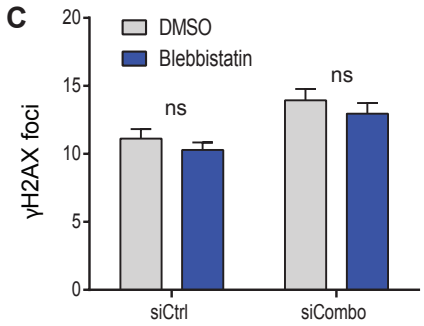

DNA repair factors (KU70/80, RAP1) interact with LMNA,
KU80 preferentially interacts with non-phosphorylated LMNA vs phospho-solubilized LMNA

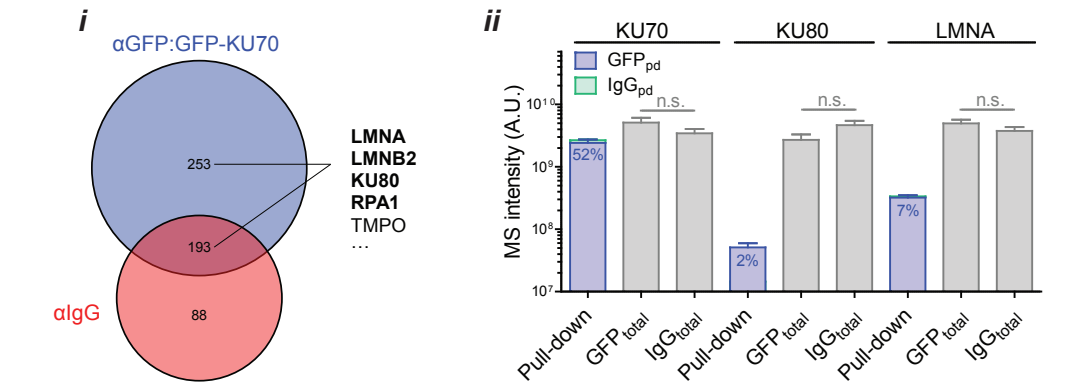

Figure S4

LMNA (but not LMNB) increases with Col1 & tissue stiffness, following a 'lose it or use it' model of tension-suppressed turnover

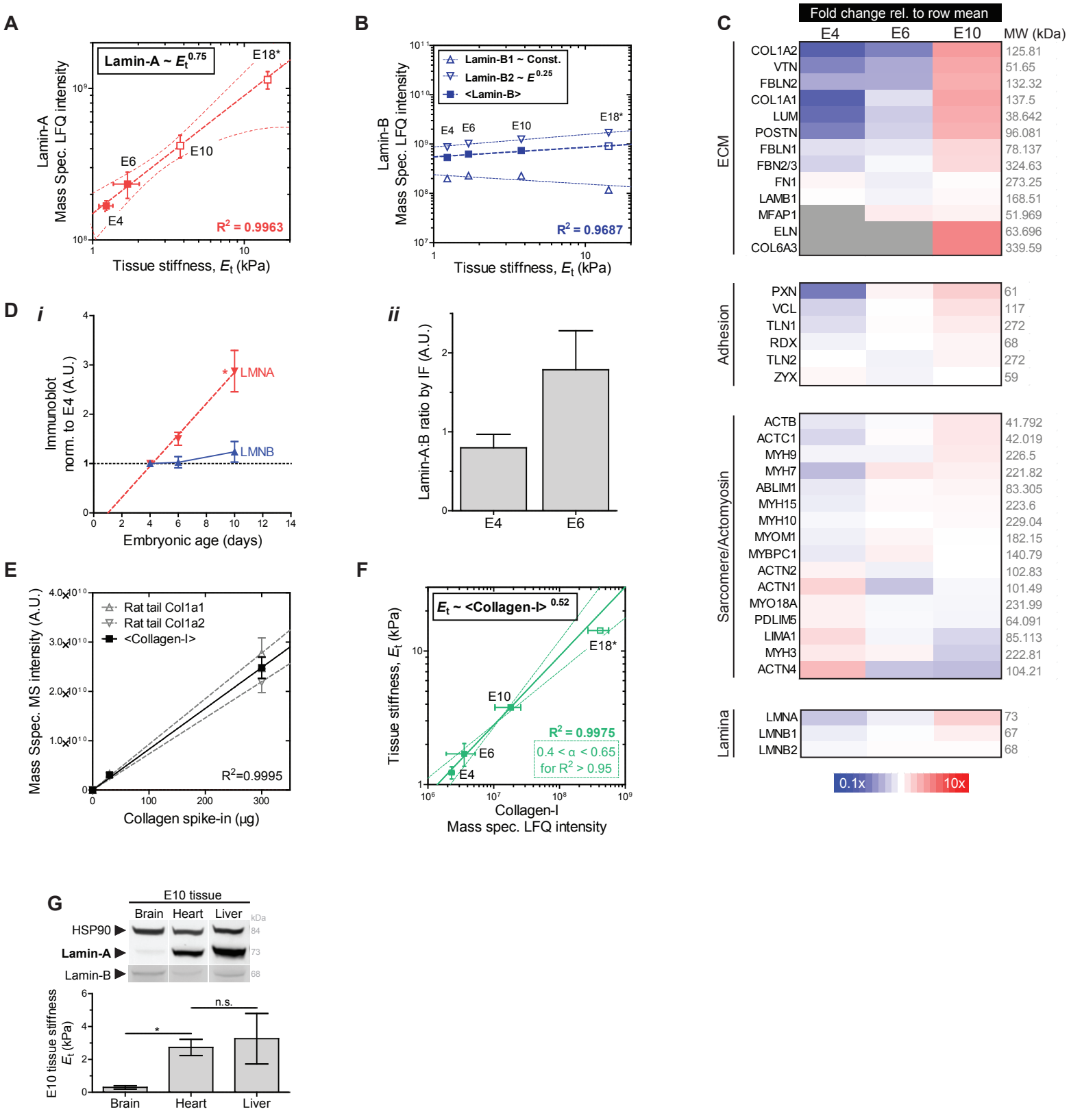

Figure S5

Reduction of stress increases phosphor. of LMNA at multiple sites

Drug perturbations do not affect repair factor RPA1 or MMP2 levels/activation

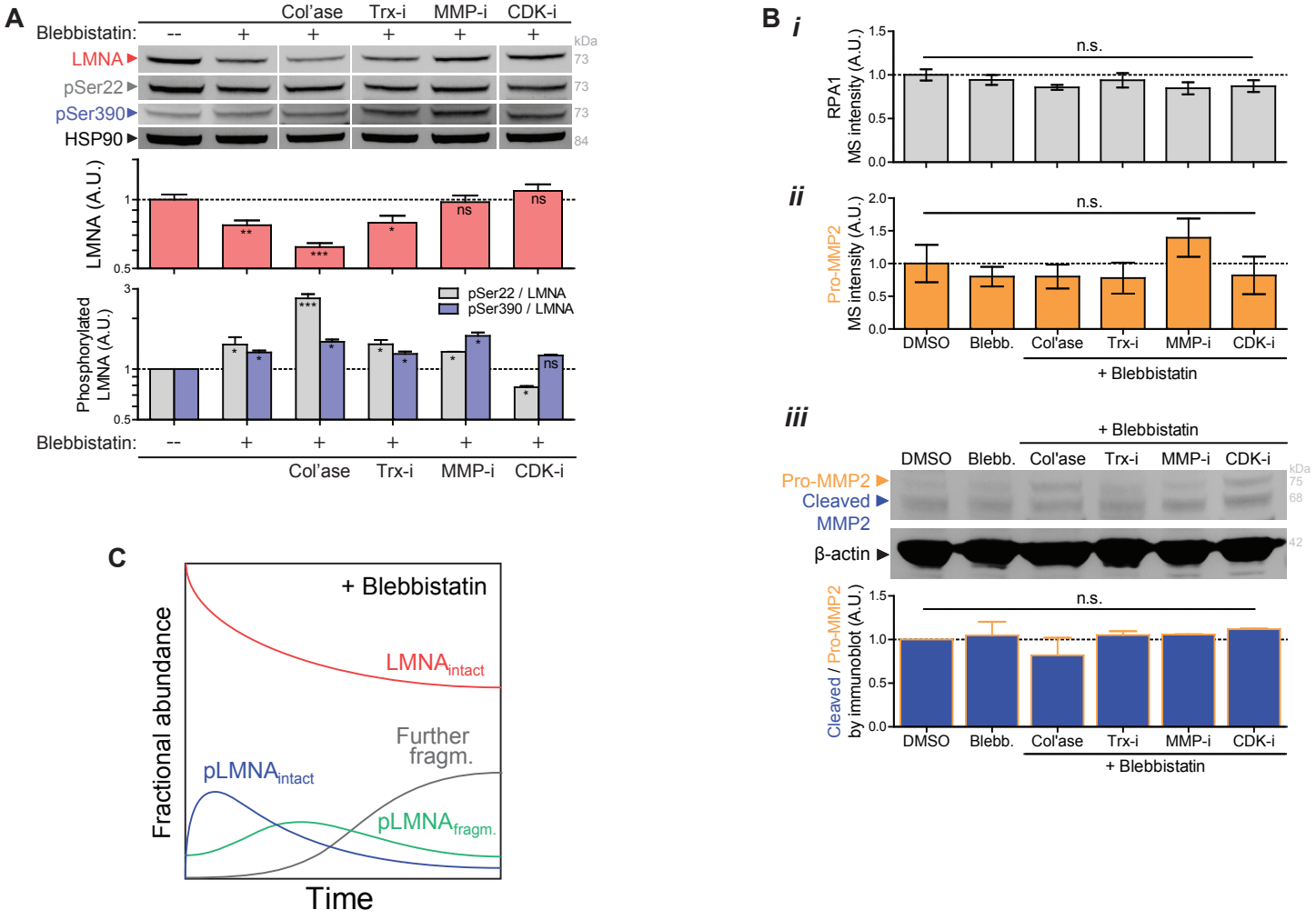

Figure S6

CMs cultured on soft/stiff Col-I-ligand gels mimic basic morphodynamics of *in vivo* development

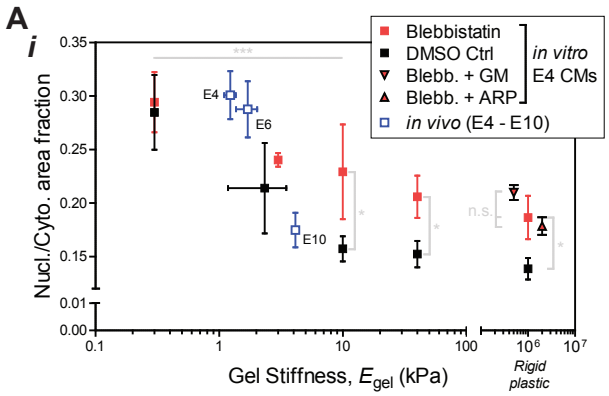

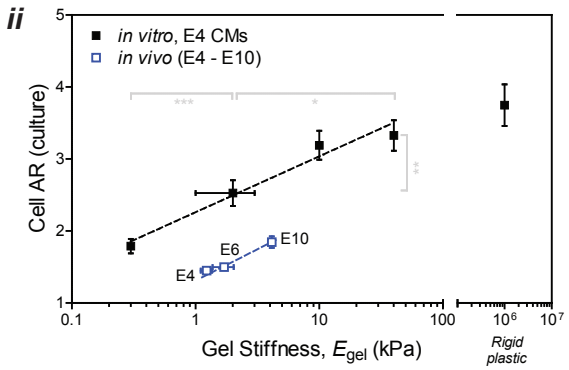

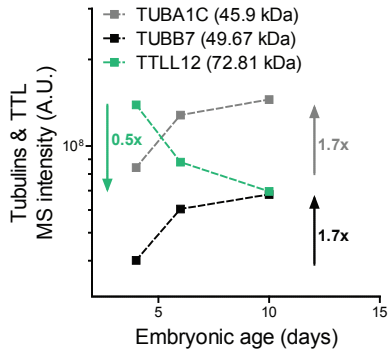

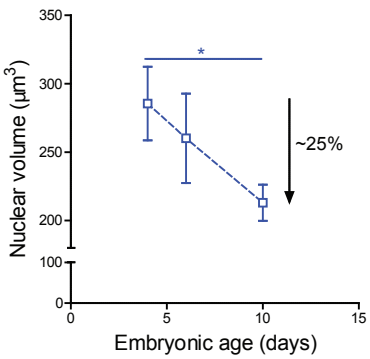

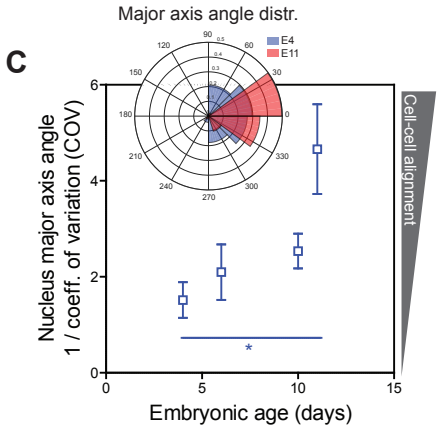

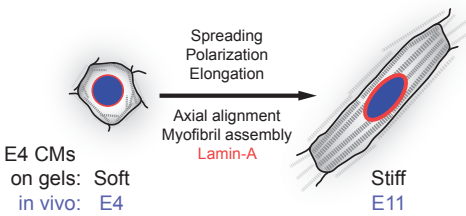

LMNA levels do not correlate with dynamic beating; instead increases with basal isometric tension

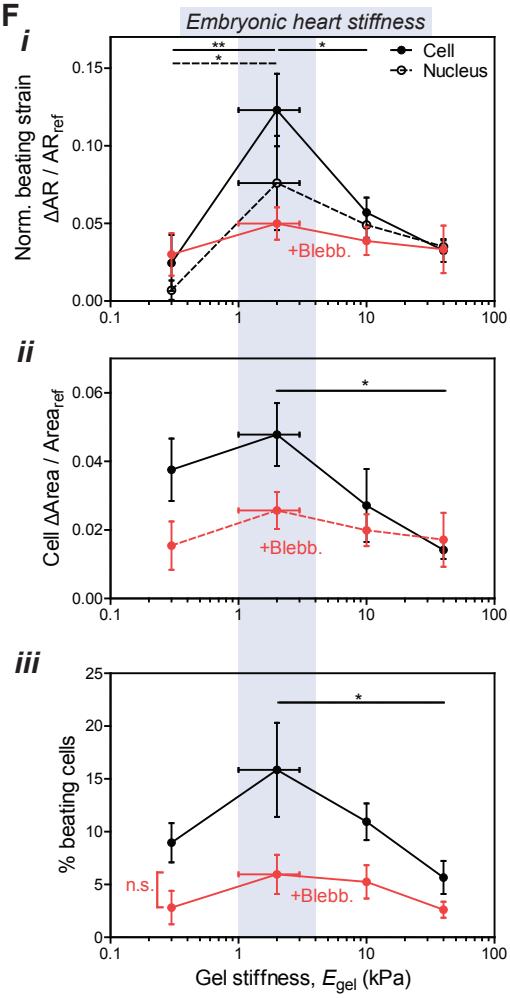

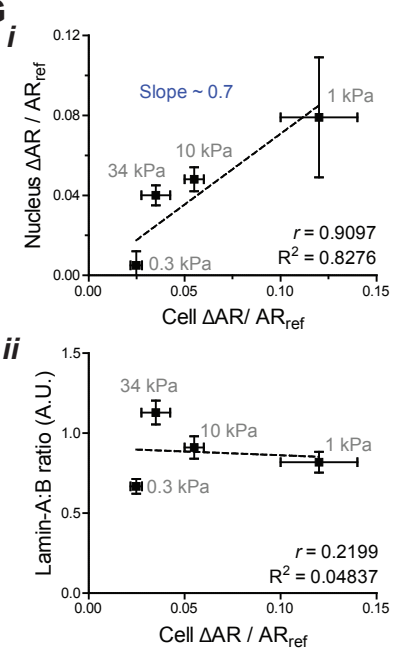

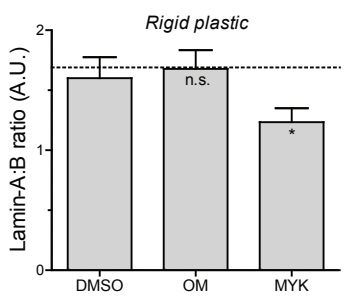

Figure S7

Phosphomimetic S22E LMNA mutant is more nucleoplasmic and more rapidly degraded than S22A

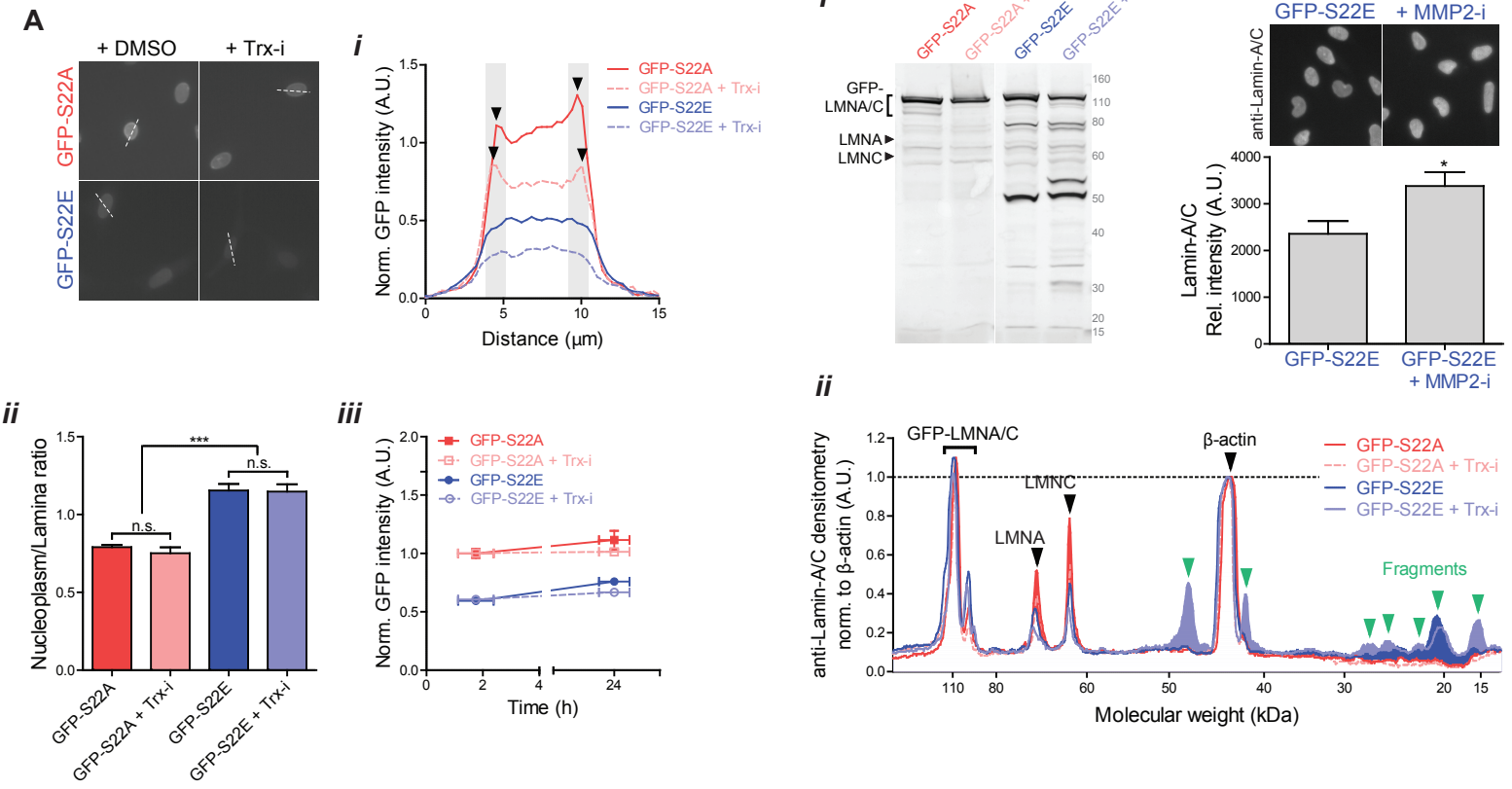

Meta-analysis of public tissue -omics databases suggests potential 'universality' of LMNA vs Col1 ECM correlations